University of North Carolina Asheville
Journal of Undergraduate Research
Asheville, North Carolina
May 2020

Site Directed Mutagenesis in the Structural Determination of F-type ATPase

Gabriel Arias
The Chemistry Department
The University of North Carolina Asheville
One University Heights
Asheville, North Carolina 28804 USA

Faculty Advisor: Dr. Ryan Steed

Abstract

Adenosine triphosphate (ATP) provides energy to all forms of life. It is synthesized by a membrane protein complex, ATP synthase, comprised of two portions, the soluble F_1 and the membrane embedded F_o. The synthesis of ATP comes about from the transformation of an electrochemical gradient which in turn facilitates mechanical energy and ultimately chemical energy once ATP is synthesized. Rotation of the c_{10} ring of the embedded F_o is a result of the electrochemical gradient created from a difference in the concentration of H^+ across the membrane between the cytoplasm and external compartment within the cell, prompted by the electron transport chain. The movement of H^+ is understood to be through half-channels within the stator of F_o. However, the detailed mechanism of the rotation of the F_o motor remains unknown. Cryogenic electron microscopy has provided medium resolution structures of F_1F_o ATP synthase, but the inconsistency between structural data and previous cross-linking data within subunit *a* suggests the existence of multiple conformations for subunit *a*. To date, both *a*Y263C and the double mutation *a*V86C/*a*L161C have been grown and utilized using site directed spin labeling (SDSL) and electron paramagnetic resonance (EPR) to probe information regarding mobility and rotameric states.

1. Introduction

F-type adenosine triphosphate (ATP) synthase (Figure 1) plays a primary role in the production of energy across all forms of life. ATP (Figure 2) creates favorable reactions by releasing energy for every phosphoryl group removed and thus functions as an energy carrying molecule. Due to the fundamental role played by this nucleotide in metabolism, understanding the synthesis of ATP would allow for a greater insight in how to combat disease and contribute to the longevity of life.

F-type ATP synthase, the primary source of ATP in cells, is comprised of the membrane embedded F_o and soluble F_1. For the model found in *E.coli*, the F_1 portion is made of the $\alpha_3\beta_3$ hexamer, δ, γ stalk and ε subunit. Recent studies also suggest an arm like motion achieved by the ε subunit that possibly forces ATP synthases into motion or inhibits ATP production through its ability to detect changes in pH and ATP concentration.[12] The membrane embedded F_o contains the c_{10} ring, b_2 stalk and subunit *a*.

The $\alpha_3\beta_3$ hexamer, contained in F_1, undergoes three conformations during synthesis, which include closed, loose and tight. In the open conformation, the space within the dimer mantains an inorganic phosphate (P_i) as well as adenosine diphosphate (ADP). Once in the tight state, it catalyzes a condensation reaction resulting in ATP.

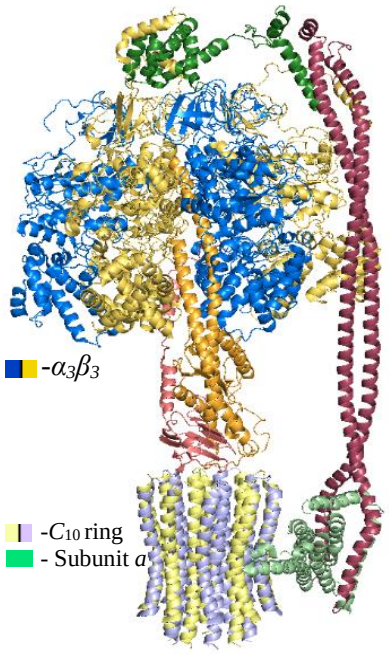

Figure 1. F-type ATP synthase

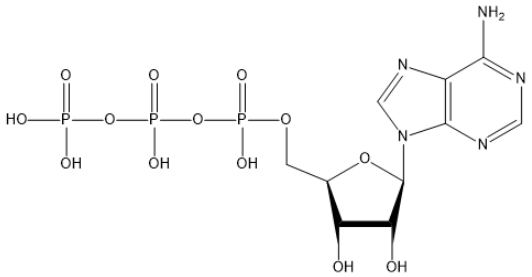

Figure 2. Adenosine triphosphate

Subunit *a* facilitates the translocation of protons through aqueous half channels separated by a highly conserved Arginine 210 located between the *a* and *c* subunits.[3] These half-channels act as channels for protons to protonate Asp^{61} on subunit *c* and, after a full counter clock-wise rotation of the rotor, enter the N-side half-channel, moving out of the protein complex into the cytoplasm.[6] The protonation of Asp^{61} within the c_{10} ring along and interactions with Arg^{210} play a key roles in subunit *c*'s rotation. Through this process the F_o motor creates mechanical energy, or torque, to revolve the F_1 motor attached through the above mentioned γ subunit. These rotations are regulated by the ε subunit.[4]

The rationale behind the importance of Arg^{210} and its regulation of protons is hypothesized in two models, the electrostatic model and the mechanical model. The electrostatic model hypothesizes that rotation is achieved due to the weak interactions between the negatively charged stator and the positively charged motor. The mechanical model suggests that the rotation of the *c* subunit comes directly from the chemical gradient and the physical interactions of *a* and *c*. The mechanical model is often considered more feasible due to the over-all high efficiency of the system.[5]

The current structural model for the whole of ATP synthase, using various instrumentation, has been developed by scientists over the course of a few decades.[6] Methods including cryogenic-electron microscopy (cryo-EM), site-directed mutagenesis and crystallography have resolved a high-resolution image of F_1 and a medium resolution image of F_o in *E.coli*.[4] However, complete structural information regarding some of the more highly conserved residues on these subunits that facilitate the rotation of subunit *c* is missing. The F_o portion being embedded means it is not as easily determined through cryo-EM, although some F_o portions contained within other ATP synthases are more easily elucidated, such as *Bacillus pseudofirmus*, an anaerobic gram positive bacteria whose *c*-subunit sticks slightly out of the membrane.[7] Fillingame and colleagues mapped the structure and translocation of H^+ through *E.coli*'s subunit *a* and *c*.[8]

The current understanding of subunit *a* does not fully account for the implied but not yet proven conformational change. The two specific aims of the group consist of the following: 1) defining the functionalities of specific residues in the rotor-stator configuration using site-directed mutagenesis; 2) utilizing site-directed spin labeling (SDSL) and electron paramagnetic resonance spectroscopy (EPR) as an approach to determine the movement or change in conformations and verifying the proposed architecture of subunit *a*.[9] SDSL-EPR utilizes radicals within (1-Oxyl-2,2,5,5-tetramethylpyrroline-3- methyl) methanethiosulfonate (MTSL) that are bounded to Cys residues, by a disulfide bond, introduced into a protein (Fig. 3) to elucidate the structural environment and its characteristics at the Cys position using the first derivative of the microwave absorption spectrum. Using the data gathered from EPR, analysis of the line width and shape of the low-field absorbance gives information pertaining to the residues' structural environment, mobility and solvent accessibility. Analyzing a multitude of residues using this method can give insight into dynamics, functionality and conformational changes that may be occurring. Identifying which residues play a role in maintaining structural integrity elucidates which aspects of subunit *a* have a direct impact on the translocation of protons. Overall,

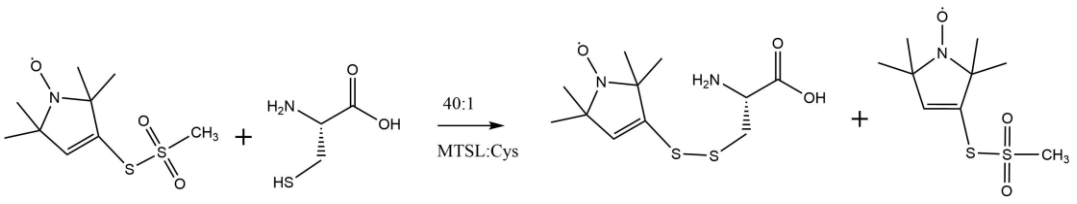

Figure 3. MTSL reaction using cysteine mutation in a 40:1 or a 20:1 reaction ratio. The abundance of MTSL is what drives the less the favorable reaction towards the desired product

the main focus of both aims is to classify, define, and depict the major roles of the residues corresponding to the F_o motor using proton pumping assays, ATP synthesis assays, site-directed mutagenesis, and EPR.

The information about F_o pertains primarily to how protons move through the subunits with a limited amount of information on how their interaction facilitates the rotation of c_{10} as a consequence of the lack of information regarding the positioning of the residues. More specifically, we know that subunit *a* uses proton translocation to transport protons from outside the cell membrane, otherwise known as the P-side, and move them towards the *a*-*c* interface. We also know the partial functionality of Arg^{210} located on the *a* subunit. This crucial residue acts as a deviator to the protons passing through subunit *a* into subunit *c*, to be attached to the Asp^{61}. The proton pumping functionality of ATPase also utilizes the half-channels in a similar fashion. Although this understanding is critical, the question of how conformational changes and electrostatic interactions play a role in the rotation of the γ stalk remains unanswered.

Our research group has to date optimized protein purification, spin labeling and efficient removal of unreacted MTSL. More recently we have been able to successfully remove free or unreacted spins using gel filtration chromatography. Through a NIH grant, the Steed lab has also afforded a new BioRad fast protein liquid chromatographer (FPLC) and a bench top EPR manufactured by EMX. This improvement to our methods, and new instrumentation, is significant in correlation to producing accurate results without contamination and within at timely manner, which will allow us to better interpret the bound spins on the targeted residues. The objective of this work generally is producing and reproducing the purification process of removing ATP synthase from *E.coli*, attaching MTSL and removing unreacted spin-labeled molecules. Figure 3 illustrates the reaction of MTSL with cysteine, thus there is the possibility that MTSL goes unreacted, which is referred to as unreacted spin-labels.

2. Material and Methods

2.1 *a*Y263C

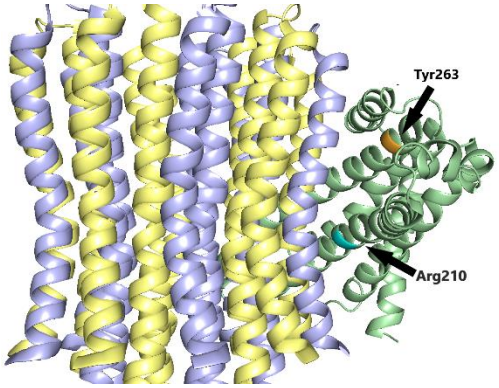

Figure 5: Location of aY263C in respects to Arg210

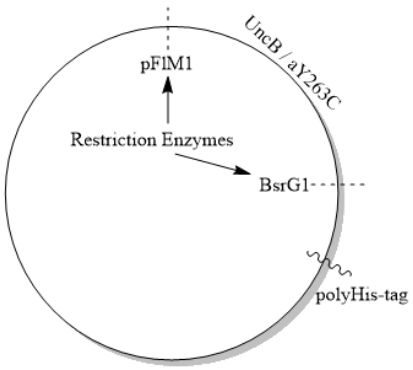

Figure 6: DNA representation of desired mutation aY263C

2.1.1 mutagenesis

A previously generated derivative of the plasmid pCMA1138 was utilized for the mutation of interest. Tyrosine, at position 263 on subunit *a* shown in figure 4 has been altered to a cysteine. Digestion of pCMA113 and pFV2 with restriction enzymes pFlM1 and BsrG1 allow us to isolate the desired portions of the DNA strand from each plasmid. The "insert" contains our *a*Y263C mutation and the "vector" contains the codon for the poly-histag on β. (Figure 6). The DNA fragments were purified using 1% agarose gel in TAE buffer (2.0 M Tris base, 100 mM Na2EDTA, Acetic acid, pH 8.6). Desired bands were cut from gel and used with an extraction kit (New England Biolabs). The resulting fragments were ligated with T4-ligase to bring together the two separate strands of DNA. DH5α cells were grown on LB agar with 100 μg/mL ampicillin and incubated at 37°C overnight. The colonies were used for the inoculation of small culture in 5 mL LB with the denser cultures later purified using a plasmid mini-prep kit (New England Biolabs). The plasmid was confirmed by DNA sequencing and transformed into DK8 cells for their absence of required ATP synthase operon. The transformed cells were stored at -80°C in a 12% glycerol solution. This solution is later used in protein purification.

2.1.2.protein purification

Small cultures of the *a*Y263C in a lysogeny broth (LB) media were allowed to incubate overnight with shaking (37 °C at 240 rpm). Small cultures were scaled up to 1 L, prepared in LB, and incubated for 8 hours (37 °C, 240 rpm). The resulting growth was centrifuged for 15 minutes at 4000 rpm. TMDG buffer (50 mM Tris, 5 mM MgCl2, 10% glycerol, pH 7.5, including 1 mM DTT to protect Cys against oxidation) was used for resuspension of the cell pellet. In order to lyse the cells, the resuspended cells were homogenized at 15,000 psi to generate inverted membrane vesicles. Cell debris was cleared from the lysate by centrifugation at 9,000 x g for 10 min, and membrane vesicles were collected from the cleared lysate by centrifugation at 198,000 x g for 60 min. The pellet from centrifugation of lysate was resuspended with an extraction buffer (5 mL 2x XWL stock (40 mM Tris, 600 mM NaCl, 200 mM sucrose, 4 mM $MgCl_2$, 20% (*w/v*) glycerol, pH 8.0), 1 M DTT, 1% DDM, 200 μL of 1 M imidazole in 10 mL total volume) and rocked for 30 minutes at 4°C. The extraction was cleared by centrifugation at 498, 000 x g for 30 min. Cleared extract was added to equilibrated Ni-NTA beads for Ni-affinity chromatography to separate F_1F_o using wash buffer (50% 2x XWL, 2% 4-aminobenzamidine, 1% DDM, .02% 1 M imidazole in 20 mL total volume) and elution buffer (50% 2x XWL, 1% DDM, 5% 1 M imidazole in 10 mL total volume). In order to determine the concentration of purified protein, a modified Lowry assay[11] was run on a Biotek synergy HTX multi-mode reader at an absorbance of 650 nm. Size exclusion chromatography was done using a Pharmacia single path monitor UV-1/214, a GE Superose 6 Increase with 10/300 GL and a mobile phase of .02% sodium azide in filtered water.

2.1.3 epr data acquisition

In order to probe the electronic environment of the spin-labeled mutated protein, the aliquots chosen from FPLC we concentrated down further. The resulting protein was then used for EPR which was performed on a Bruker EMX EPR with win-EPR software, afforded by Clemson University prior to acquiring the EMXnano. A 100-gauss scan was performed on the samples at varying pH. The first scan was purified protein aliquot at a pH of 8 and acquired using 36 scans. The second pass utilized the same number of scans but 1 M MES was added in order to lower the pH to around 5.

2.2 *a*V86C/*a*L161C

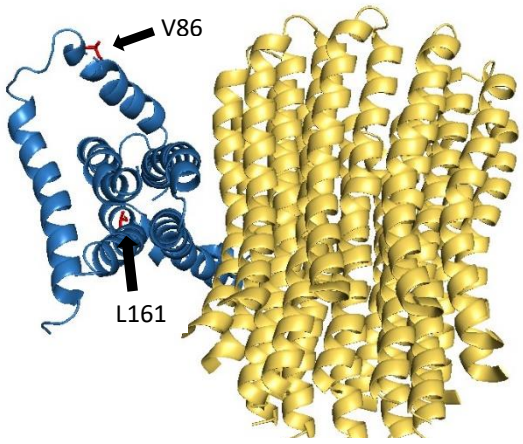

Figure 4. Location of V86 and L161, in red

2.2.1 mutagenesis

A previously generated derivative of the plasmid pFV2 was utilized for the double mutation of interest. Valine, at position 86 as well as leucine, at position 161, were both altered to a cysteine. These cysteine mutations contain thiol functional groups and thus allow for the disulfide bonds responsible for reacting the spin label. Plasmid pFV2[10] contains a poly-histidine tag located on subunit β for coordination with Ni-NTA in our affinity chromatography necessary for detachment of F_1F_0 from other proteins. This double mutation was already a part of the lab's library of

mutated *E.coli* strains; thus, mutagenesis had already been completed prior and the samples were stored at -80° C in a glycerol stock.

2.2.2. protein purification

The same protocol was utilized for the double mutation as was *a*Y263C. The amount of MTSL was reconsidered to lower the concentration of unreacted spin post-FPLC. The concentration was verified and a 20:1 ratio of MTSL to protein was added.

2.2.3 spin-labeling and size exclusion chromatography (sec)

Once the concentration was verified, a molar excess of MTSL to protein (20:1) was added. Lower ratios may help reduce the amount of free spin remaining after FPLC. The reaction incubated at room temperature for 60 min, and a second shot of MTSL was added to drive the reaction to completion and incubated overnight on ice. Spin-labeled protein was run through SEC using a Superose 6 10/300 column on a Bio-Rad NGC Quest 10 to obtain the desired population of protein and aid in removal of unreacted MTSL.

2.2.4 epr data acquisition

The spin-labeled protein was the concentrated to 100 µL using a spin concentrator with 100 kDa molecular weight cutoff. A 100-gauss scan was performed, using an EMXnano, on the samples at varying pH. The first scan was purified protein aliquot at a pH of 8 and acquired using twenty-five 90 second scans, with a modulation amplitude of 1.2 G and a microwave power of 10 mW. The second pass utilized the same number of scans but 1 M MES was added in order to lower the pH to around 5. The EPR data acquired contains more free spin label for pH 5 since the run was done a day later using the same protein.

3. Results and Discussion

3.1 *a*Y263C

Protein ladder used to verify number of KDa

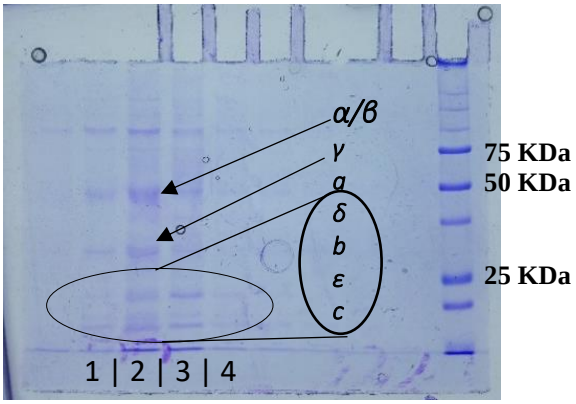

Figure 10. SDS-Page gel with elution aliquots and protein marker

3.1.1 preparation of mutation

An integral step within the preparation of the enzyme is affinity chromatography using Nickel-Nitrilotriacetic acid (Ni-NTA) resin. This resin consists of very small beads that bind to the poly-histag spoken of prior. This affinity chromatography is used to separate the enzyme from debris generated post-homogenizing. To verify the protein is present in full, and SDS-PAGE gel is used to examine the usually 10 aliquots from the elution step within the affinity chromatography protocol. Of the ten samples from SDS-PAGE gel, four showed signs of the separated protein of

interest present (Figure 10). This gel shows the presence of the individual segments of ATP synthase and verify our enzyme is present in completion. Subunit a is often to faint to recognize and is over-shadowed by subunit γ. Fractions 1-4 were pooled to undergo FPLC.

3.1.2 fplc data

The graph generated from FPLC during this procedure differs in its response, volts (V) vs time. This procedure was done twice. Before acquiring the NIH grant, the procedure had to be well timed and efficient. Clemson University often allowed us to use their EPR. Because of this, the window of time available for EPR spectroscopy was short, and the procedure had to be done within a weeks' time prior to arriving at Clemson. Because of this time constraint, it was often useful to do a trial run for several reasons. Ensure all equipment was working properly, too assure the enzymes feasibility for spin-labeling, and to have a more accurate representation of the time needed to complete each step leading up to transportation to Clemson.

In this report, there are two graphs, one from the trial run (Fig 11, graph A), and the other for the sample that would later be transported to Clemson (Fig 11, graph B). Results for both graphs contain multiple peaks, indicative of degradation or deterioration of the protein after affinity chromatography which can be seen in both graphs contained in figure 11. There are many possibilities as to why our protein may have separated. The initial purification produced, at a high concentration, a skewed graph with multiple underlying peaks. The second purification was determined to be a low concentration with several peaks. We can conclude from the initial purification process that our mutation,

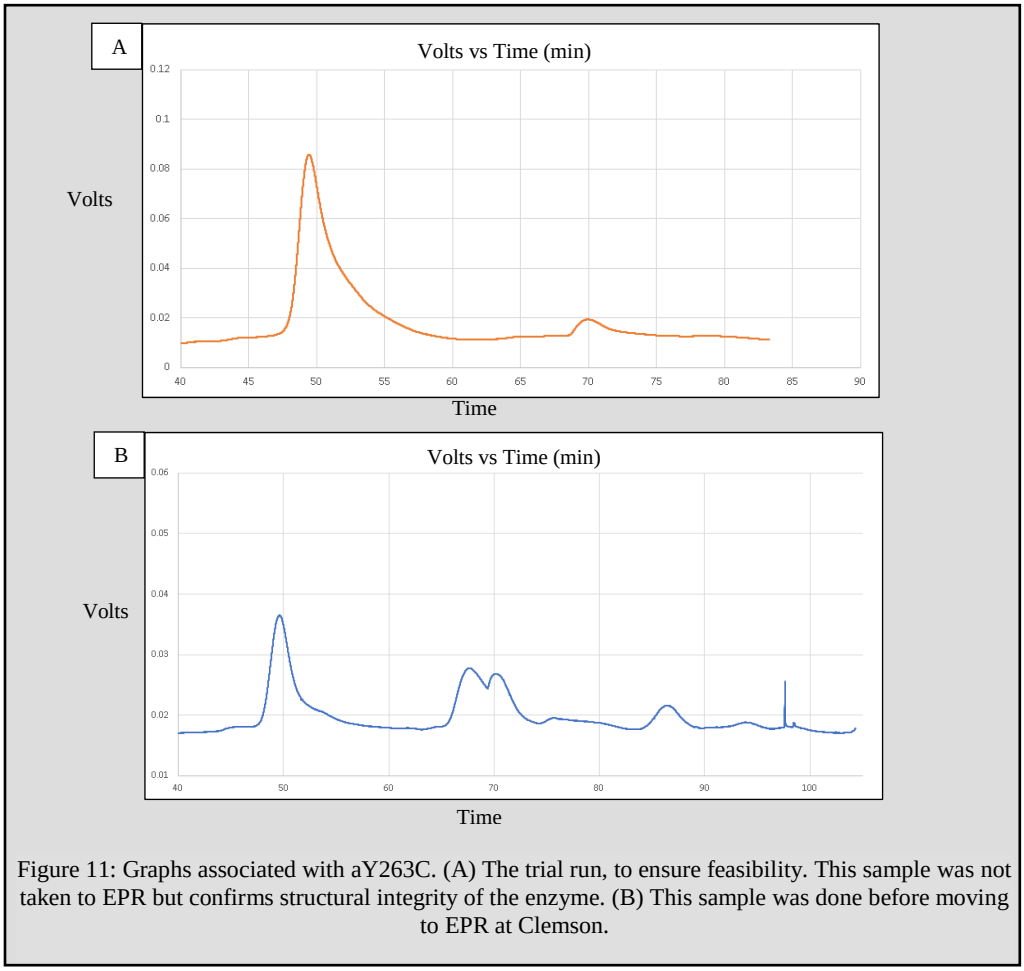

Figure 11: Graphs associated with aY263C. (A) The trial run, to ensure feasibility. This sample was not taken to EPR but confirms structural integrity of the enzyme. (B) This sample was done before moving to EPR at Clemson.

along with our procedure, does not structurally compromise ATP synthase because there is still a monodispersed population. In graph B, the first peak is the void volume. Due to a higher protein concentration in graph A, this void volume is minimized as noise. The second portion of the combined peaks in graph B is considered to be the enzyme. The rest is debris or portions of the enzyme that did not hold well.

3.1.3 epr data

The protein utilized for spin labeling (Graph B) was present at a low concentration, thus the resulting EPR data contained a low signal to noise ratio present in the EPR graph of figure 12 making any sort of conclusion difficult from just this data (Graph B). There are some points of interest that make this experiment viable for re-examination. The left side of the center line corresponds to the lower magnitude magnetic field, which shows the most apparent difference. The shift in peaks as well as the difference of slope leading up to this first peak also differs with pH, thus a conclusion could be made in regards into differing rotameric states available to these residues upon a change in pH. Results from data gathered are not necessarily indicative of a dynamic subunit. Further examination of this mutation and others could elucidate a possible trend in the shifting of these bonds, giving greater insight to whether or not subunit a is in fact dynamic, and if so, in what ways.

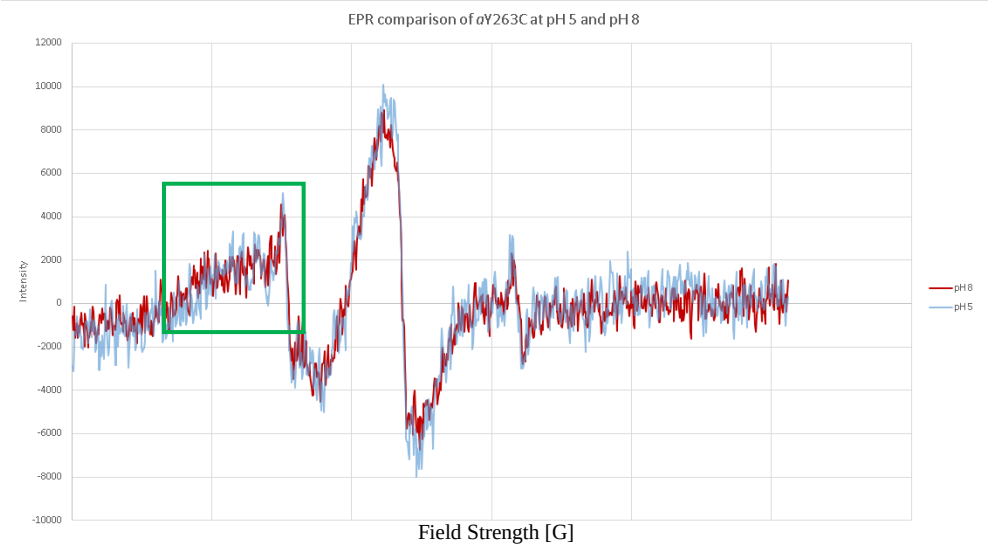

Figure 12: EPR data acquired with the *a*Y263C mutation. Within the green rectangle is the difference in slope that corresponds to a possible change in rotameric states.

3.2 *a*V86C/*a*L161C

The objective of this method is to utilize EPR to observe the electronic environment and how it may vary with a change in pH. Because ATP synthase's functionality arises from the proton gradient across the membrane, it is thought by varying the pH, conformational change may be induced. Both SDSL and utilizing MTSL for information regarding electronic environment have been used in the past to observe other enzymes but utilizing EPR on ATP synthase is novel.

3.2.1 fplc data

Size exclusion chromatography separates our protein from smaller debris and often times produces an early elution

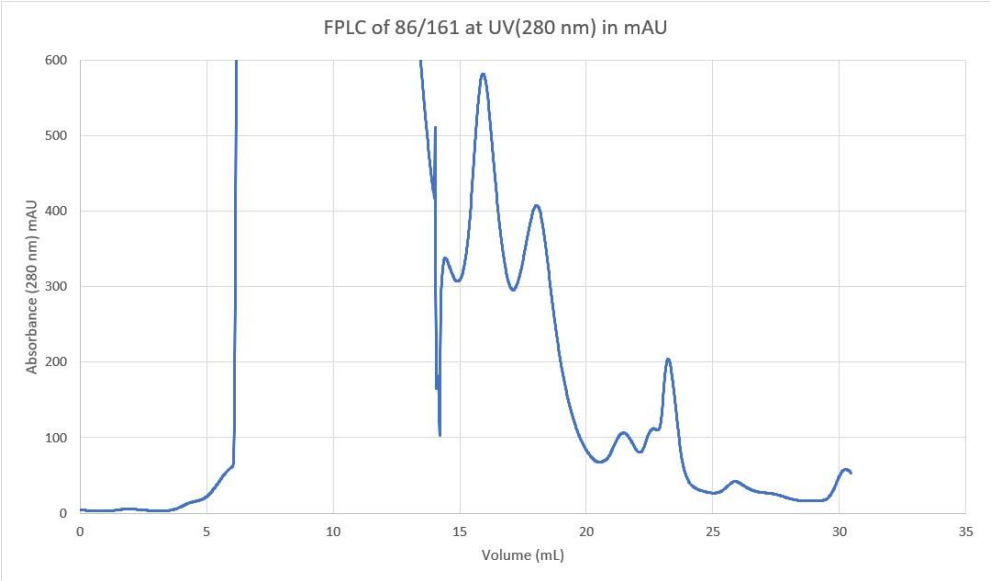

Figure 7: FPLC data acquired after spin-labeling of V86C and L161C

containing protein aggregates due to quick movement through the column. This elution typically occurs around 8 mL of column volume and is considered a void volume, which will be more prevalent in the graph pertaining

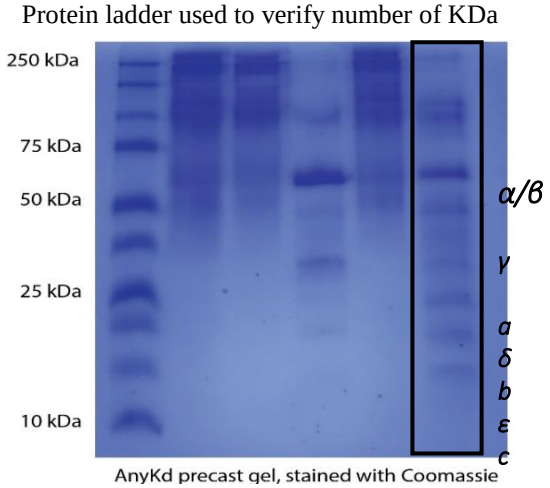

Figure 8: SDS-Page gel with elution aliquots, the boxed lane is associated with aliquots at 16-17 mL from the FPLC chromatogram

to *a*Y263C. The graph in figure 7 is produced from FPLC. It is shown as a A_{280} vs volume (mL) plot that ideally produces a monodispersed population indicative of a homogenous solution during elution. Unfortunately, during this process, an air pocket became trapped within the UV detector, though the expected peaks did come after. The leveled off peak within 6 to 12 mL is indicative of the air pocket. Because these procedures have been done numerous times within the lab, successfully with other mutated enzymes, the aliquots of interest do not typically change due to the nature of SEC. Therefore, although the air pocket disrupted our data, it is still understood that the aliquots of interest typically lie around the 14-19 mL range of elution. Following the removal of the air pocket, the elution volumes

correlating to12-19 were the volume of interest. In order to confirm which aliquots contain the desired population an SDS-page gel is run on a small sample from each aliquot of interest to probe which subunits are present. After seeing the page-gel (Fig 8) the aliquots correlating to the elution at 16-17 mL were chosen for EPR. The rest was determined to be debris or portions of the enzyme that did not hold well.

3.2.2 epr data

Figure 9 is the data generated from the double mutation aliquots 14-15. The main characteristic that is of interest with these experiments is what is known as distance from the center line. The first sharp peak that occurs at around 3420 G is the peak associated with mobility. The data represented here is of the mutation at multiple pH's, 8 and 5. Upon the introduction of 1M MES, there seems to be no obvious shift in the peak location in regard to the distance from the center line, around 3430 G. There is one distinguishable characteristic of both curves. The intensity of the scan leading up to the first peak differs in slope. That is, the rate of change is drastically steeper for the double mutation at a pH of 5, which may indicate a possible change it rotameric states, a rotation in the bonds, that changes the residues conformation at either one or both of these positions.

4. Conclusion

The novel approach at elucidating the dynamic functionality between the *a*-*c* interface is a multi-level process utilizing protein purification, site directed spin labeling and EPR. A practical use to the information gathered is to further our understanding of essential H^+ binding occurring around the *c*-subunit Another interesting field of study is just how ATPase utilizes the electromagnetic field to "decide" when it must proton pump rather than synthesize, commonly seen in other forms of the enzyme and how the ε subunit knows when to interfere with the $\alpha_3\beta_3$ hexamer responsible for synthases. Since ATP synthase is found in all cells, regulates pH and is synthesizing an energy carrying molecule later utilized in metabolism and the electron transport chain, furthering our understanding and identifying what drives this marvelous enzyme would not only contribute to science but would aid in the combat against diseases like *Mycobacterium tuberculosis.* This specific strain of mycobacterium is notorious for being a multi-drug resistant infection having killed millions.[12]

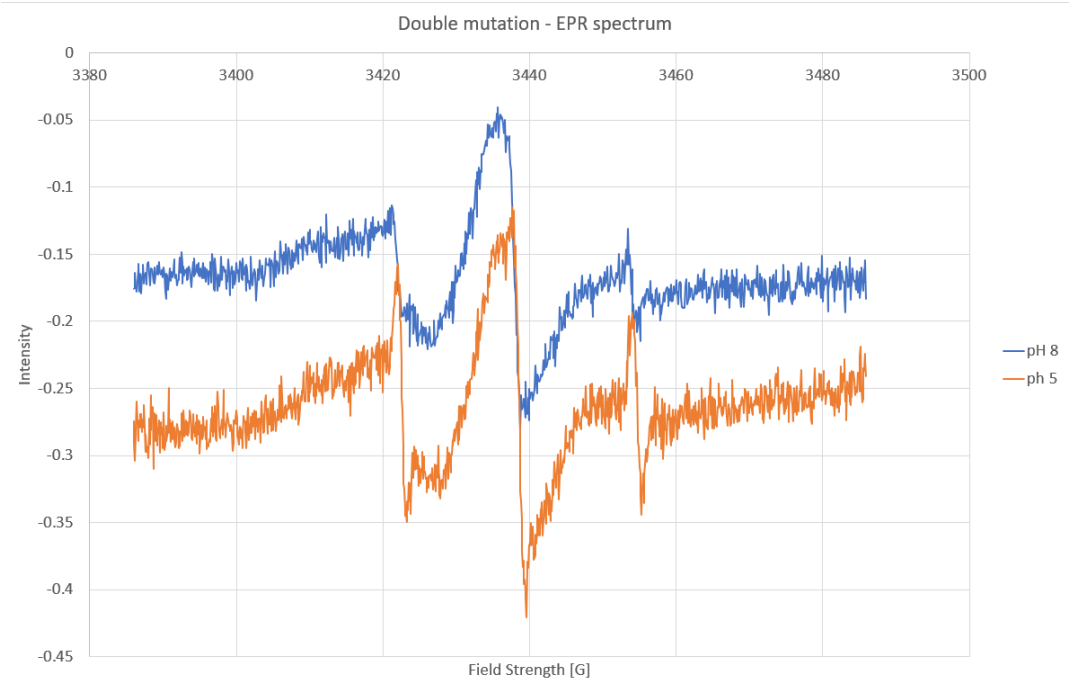

Figure 9: EPR data acquired from aliquots 14-15 at different pH's. Blue corresponds to pH 8 and orange pH 5.

In order to characterize any dynamic shifts, this procedure must be done with many mutations. The most important aspect of this is discovering a trend in mobility and shifts in electronic environment. An interesting topic is the discussion of the electrostatic field in respects to mutated residues and how it effects synthesis activity. All of these questions along with multiple spin-labeled mutations will give insight to the conformational nature of the *a-c* interface and possible contribute to the discussion on how ATP synthase is able to utilize the proton gradient to create the torque necessary to induce the conformational changes within F_1.

Furthermore, characterizing the different types of ATP synthase found between bacteria and cells and understanding how each nucleotide contributes to its model of ATP synthase may lead to information on to competitively or noncompetitively inhibit ATP synthase. is ultimately the end goal. Because F-type ATP synthase found in *E.coli* is easily grown and is one of the simpler forms of ATP synthase, our interest lies in uncovering the secrets of this evolutionary phenomena as a stepping stone towards understanding the larger complexes such as V-type ATP synthase or the dimerization. The future direction of the lab includes further characterization of the different single and double mutation using proton pumping and ATP synthases assays to verify functionality as well as reconstituting the cells to get an even more accurate representation.

5. References

1. Joon, S.; Ragunathan, P.; Sundararaman, L.; Nartey, W.; Kundu, S.; Manimekalai, M. S. S.; Bogdanović, N.; Dick, T.; Grüber, G. The NMR Solution Structure of Mycobacterium Tuberculosis F-ATP Synthase Subunit ε Provides New Insight into Energy Coupling inside the Rotary Engine. *FEBS J.* **2018**, *285* (6), 1111–1128. https://doi.org/10.1111/febs.14392.
2. Sielaff, H.; Duncan, T. M.; Börsch, M. The Regulatory Subunit ε in Escherichia Coli F O F 1 -ATP Synthase. *Biochim. Biophys. Acta - Bioenerg.* **2018**, *1859* (9), 775–788. https://doi.org/10.1016/j.bbabio.2018.06.013.
3. Leone, V.; Faraldo-Gómez, J. D. Structure and Mechanism of the ATP Synthase Membrane Motor Inferred from Quantitative Integrative Modeling. *J. Gen. Physiol.* **2016**, *148* (6), jgp.201611679. https://doi.org/10.1085/jgp.201611679.
4. Sobti, M.; Smits, C.; Wong, A. S. W.; Ishmukhametov, R.; Stock, D.; Sandin, S.; Stewart, A. G. Cryo-EM Structures of the Autoinhibited E. Coli ATP Synthase in Three Rotational States. *Elife* **2016**, *5* (DECEMBER2016), 1–18. https://doi.org/10.7554/eLife.21598.
5. Matta, C. F.; Massa, L. Energy Equivalence of Information in the Mitochondrion and the Thermodynamic Efficiency of ATP Synthase. *Biochemistry* **2015**, *54* (34), 5376–5378. https://doi.org/10.1021/acs.biochem.5b00834.
6. Srivastava, A. P.; Luo, M.; Zhou, W.; Symersky, J.; Bai, D.; Chambers, M. G.; Faraldo-Gómez, J. D.; Liao, M.; Mueller, D. M. High-Resolution Cryo-EM Analysis of the Yeast ATP Synthase in a Lipid Membrane. *Science (80-.).* **2018**, *360* (6389). https://doi.org/10.1126/science.aas9699.
7. Preiss, L.; Yildiz, O.; Hicks, D. B.; Krulwich, T. A.; Meier, T. A New Type of Proton Coordination in an F(1)F(o)-ATP Synthase Rotor Ring. *PLoS Biol.* **2010**, *8* (8), e1000443. https://doi.org/10.1371/journal.pbio.1000443.
8. Steed, P. R.; Fillingame, R. H. Aqueous Accessibility to the Transmembrane Regions of Subunit c of the Escherichia Coli F1F0 ATP Synthase. *J. Biol. Chem.* **2009**, *284* (35), 23243–23250. https://doi.org/10.1074/jbc.M109.002501.
9. Claxton, D. P.; Kazmier, K.; Mishra, S.; Mchaourab, H. S. Navigating Membrane Protein Structure, Dynamics, and Energy Landscapes Using Spin Labeling and EPR Spectroscopy. *Methods Enzymol.* **2015**, *564*, 349–387. https://doi.org/10.1016/bs.mie.2015.07.026.
10. Ishmukhametov, R. R.; Galkin, M. a; Vik, S. B. Ultrafast Purification and Reconstitution of His-Tagged Cysteine-Less Escherichia Coli F1Fo ATP Synthase. *Biochim. Biophys. Acta* **2005**, *1706* (1–2), 110–116. https://doi.org/10.1016/j.bbabio.2004.09.012.
11. Fillingame, R. H. Identification of the Dicyclohexylcarbodiimide-Reactive Protein Component of the Adenosine 5'-Triphosphate Energy-Transducing System of Escherichia Coli. *J. Bacteriol.* **1975**, *124* (2), 870–883.
12. Preiss, L.; Langer, J. D.; Yildiz, Ö.; Eckhardt-Strelau, L.; Guillemont, J. E. G.; Koul, A.; Meier, T. Structure of the Mycobacterial ATP Synthase Fo Rotor Ring in Complex with the Anti-TB Drug Bedaquiline. *Sci. Adv.* **2015**, *1* (4), e1500106. https://doi.org/10.1126/sciadv.1500106.